Copyright © 1997 Elsevier Science Ltd
Int. J. Rock Mech. & Min. Sci. Vol. 34, No. 3-4, 1997 ISSN 0148-9062
To cite this paper: *Int. J. Rock Mech. & Min. Sci.* **34:3–4**, Paper No. 292

HYDRODYNAMIC EROSION; A POTENTIAL MECHANISM OF SAND PRODUCTION IN WEAK SANDSTONES

A. Skjærstein[1]; M. Stavropoulou[2]; I. Vardoulakis[2]; J. Tronvoll[1]

[1] IKU Petroleum Research, Trondheim, Norway

[2] National Technical University of Athens, Greece

ABSTRACT

Fluidized column experiments have been performed, where a 10 cm in diameter and 15 cm high cylindrical sand column was subjected to linear upwards flow of water. The tests were monitored by means of an X-ray CT-scanner. The experiments showed that a change in the flow rate gave rise to a propagating density wave starting upstream at the bottom of the sand body propagating to the top. The experimental observations have been used to calibrate a model which describes erosion processes. Flow rate changes were best described by a temporary change into mildly turbulent flow conditions, which leads to mobilisation of sand particles.

KEYWORDS

X-ray CT • Density • Erosion • Fluid flow in porous media • Modelling • Permeability • Hydrodynamics • Sand production

INTRODUCTION

Advanced numerical models may be applied to predict onset of sand production during production of hydrocarbons, but most of them are unable to give reliable quantitative volumetric estimates of sand production and post-failure behaviour of the rock. In this regime the rock matrix may have been subjected to a significant degree of softening, or at least decohesioning, the fluid flow appears to be of importance for sand production and evolution of the failure zone (Tronvoll 1993). This study was thus initiated to investigate some hydrodynamic aspects of sand production.

Conceptually, sand production can be related to two fundamental destabilization mechanisms: First, mechanical instabilities lead to localized failure of the rock. Second, dynamic drag induced hydrodynamical instabilities lead to internal and surface erosion, which manifest themselves in releasing and transporting particles (Vardoulakis *et al.* 1996). Internal erosion may be related to micromechanical impacts imposed on the solid skeleton as a result of the combined action of viscous shear through mobile solids in the pore network, gas bubbles, water droplets, etc. Surface erosion is thought of being due to the combined effect of parallel flow scouring of a free surface and normal flow over the surface. The subject of this study is the effect of fluid flow normal to the free surface.

The rock destabilisation mechanisms are coupled to each other, since stress concentrations lead to localized damage, which increases the amount of decohesioned material. The decohesioned matrix of

sand particles may in turn be mobilized by the relatively weak hydrodynamical forces. This study is consequently addressing the destabilisation mechanisms through fluidized column experiments on sand. The experiments were performed with the major purpose to observe phenomenologically mobilisation mechanisms in the sand.

A second objective of the experiments was to validate and calibrate a model for erosion kinetics in sand (Vardoulakis *et al.* 1996). The model decribes hydrodynamical instabilities that lead to surface erosion. All deformation and strength characteristics of the rock are suppressed, and the emphasis is solely on mass transport. This means that a cohesionless material as loose sand is considered. Therefore an experiment was designed for linear flow in unconsolidated sand.

EXPERIMENTAL SET-UP

The experimental set-up is illustrated in Figure 1. The set-up consists of a perforated piston at bottom and a cylindrical plexi-glass sleeve for visual observations of deformations in the sand. The diameter of the sleeve is 100 mm. The sleeve is filled with a sequence of gravel, sand, and water. Both the sand and the gravel are fully saturated when the test starts. Water is circulated upwards through the bottom piston and is thereafter distributed by the gravel, before it flows axially upwards into the sand body. The gravel used has a mean grain size of 400 μm - 430 μm. The hydrostatic pressure measured at the fluid inlet was taken as the 'zero' level. Second, the flow rate was increased in steps. The flowrate was manually measured at the outlet, with an accuracy of ±1 ml/min. The pressure was measured with an accuracy of ± 0.005 bar. The height of the sand column was measured from the X-ray CT scans, with an accuracy of ±0.5 mm.

In addition to the visual observations, X-ray Computer Tomography (CT) was used interactively to monitor sand body deformation. The scanner is based on a rotating tube detector system. The computer tomogram gives a matrix with a limited number of picture elements. The unit of the computer tomogram determines its spatial resolution. CT cross sections were created with a 1 mm separation, and the resolution obtained was (0.55*0.55*1 mm^3). Each volume element has a numerical value representing the mean attenuation in the volume element. The material density value stands in a linear relationship to the attenuation coefficient. For each flow rate level several images were taken of the sample. These images showed density changes inside the sand body due to variations of the fluid pressure gradient.

TEST RESULTS

Two different types of sand were used in the fluidized column experiments. The first one was a Danish beach sand with a mean grain size of about 160 μm, and the second called Valøygrind sand, showed a mean grain size of about 150 μm. The main difference between these two grain size distributions is that the Danish beach sand does have a smaller grain size spectrum. The beach sand exhibits a homogeneous grain size and shape (rounded), while the Valøygrind sand consist of angular and elongated grains. During the test, an equilibrium density and length of the sand column was reached for each flow rate. However, using the images, it was possible to obtain information about the process prior to equilibrium. The results from one test are given in terms of flow rate, dynamic inlet pressure, height of sand body, and 'CT-density' as functions of time. The ‘CT-density’ number is a number on the so-called Hounsfield scale, which is in linear relationship with the physical density with dimension [g/cm^3].

Based on the values of flow rate and dynamic inlet pressure, the permeability of the sand was calculated by means of Darcy's law assuming a homogeneous sand body. The results are presented in Figures 2 for the test on the Danish Beach sand and the Valøygrind sand. The permeability in Danish beach sand

ISSN 0148-9062

To cite this paper: Int. J. Rock Mech. & Min. Sci. 34:3-4, paper No. 292.

seems to be more or less constant, while the permeability seems to decrease slightly with increasing flow-rate in Valøygrind sand (Figure 2). This trend is the same as observed in the fluidized column tests outside the CT-scanner.

The mean density of the sand body was calculated from the CT-images. Density variations with time in the two tests on Danish beach sand and Valøygrind sand are presented in Figure 3. From the plot it can be seen that the initial density is higher for Valøygrind sand than for Danish beach sand. The density of the sand body remains more or less constant up to a certain flow rate, after which it starts to decrease. This critical flow rate is lower in Valøygrind sand than in Danish beach sand. In this part of the test the relationship between flow rate and density seems to be the same for the two sands. The density values presented could in principle be translated to real density values, but due to artefacts this would not give right numbers.

Fluidized column tests inside the CT-scanner, as well as preliminary tests carried out with manual column height measurements, showed that an equilibrium height was reached shortly after an increase in the flow rate. However, a significant transition regime between subsequent equilibria was experienced, and the test can consequently be divided into a transient and a steady state regime. Figure 4 illustrates schematically the transient deformation of the sand body between two equilibrium flow rates.

CT-images taken at constant flow rate in the transient regime illustrate the behaviour of the sand body. The images show a process which could be explained as a wave motion (see Figure 5). A change in the flow rate gives rise to an upwards propagating density wave in the sand body. When the wave reaches the top of the sand body a new equilibrium is reached. This wave motion was only observed for one flow rate change in the test on Danish beach sand, while the wave was seen for all flow rates in the Valøygrind sand. The reason for this difference was probably the relatively lower density contrast inside the sand body in the case of Danish beach sand as compared to the Valøygrind sand (possibly due to the differences in the grain size distribution). An additional test was performed in Danish beach sand, where the flow rate was increased from zero to maximum in one step. In this test the density wave was observed. This test also showed that the amplitude of the density wave is related to the change in the flow rate. It is possible that the density wave is appearing at all changes in flowrate in the first test on Danish beach sand, but the density contrast is too small to be observed within the resolution of the scanner. The amplitude of the density wave is determined as the density difference between the wave front and the sand body. The density variations inside the sand body as function of time were quantified for the second test on Danish beach sand by means of a mean density value as function of sand height. From the calculations it was seen that the density is lower in the parts of the sample where the wave has past through than in the remaining part of the sample. This fact is illustrated in Figure 6, where the plots show the calculated CT-density as function of the height in the sand body for two different images.

MODELLING AND BACKANALYSIS

The experiment yields at selected times t_i, where equilibrium is reached, the values of the pressure difference Δp, the flow-rate q, and the height H of the specimen. Knowing the initial porosity, $\varphi=\varphi_i$, the porosity at any time step is estimated by,

$$j = 1 - (1 - j_0)\frac{H_o}{H_i} \qquad H_0 = H_{t=0} \qquad H_i = H_{t=t_i} \tag{1}$$

ISSN 0148-9062

The density numbers given by the X-ray CT-scanner are translated to normal density (linear transformation) using the fact that the scanner is calibrated to give the value 0 for water and -1000 for air, and by taking into account the initial porosity and the bulk density of the quartz-particles (ρ_s=2650 kg/m^3).

Calibration of fluid flow law

It was found that Forchheimer's extension of Darcy's law best fits the data. In this case the governing equation for fluid flow in the considered vertical column is (cf. Vardoulakis , Sulem 1995)

$$-\frac{\partial p}{\partial z} = aq + bq^2 \qquad \text{with} \qquad a = a(\varphi) = \frac{\rho_w g}{k_w} = \frac{\rho_w \eta_k}{k(\varphi)}, \qquad b = b(\varphi) \tag{2}$$

where η_k is the kinematic viscosity of the fluid, ρ_w its density and k_w is the permeability of the medium. The left-hand-side of Eqn. 2 is evaluated from the data by setting for the hydraulic gradient $I = (-\partial p/\partial z) \approx (\Delta p/H_i)$. Forcheimer's law is validated by plotting I versus q, as shown in Figure 7.

For the determination of the permeability first the Carman-Kozeny equation was tested. The experimental data, however, suggested for the hydraulic resistivity a simple, linear in φ, law: $(1/k)=B\varphi+A$

Definitions and balance equations

The mathematical model of erosion kinetics consists of a mass balance equation and a constitutive law for particle transport (cf. Vardoulakis , Stavropoulou , Papanastasiou 1996). The approach is based on a three-phase mixture theory for a continuum consisting of skeleton solids (s), fluidized-solids (sf) and fluid (f). Fluidized-particles are particles in suspension that move with the fluid. Any other loose particles which are trapped inside the void space are seen as part of the solid phase. Moreover, it is assumed that fluid and fluidized particles share at any instance the same velocity. The solid is assumed to be rigid. In other words a solid particle has either zero velocity and is assigned to the solid phase, or it has the velocity of the fluid and is assigned to the mixture which fills the void space. The volume fraction of voids is expressed by the bulk porosity φ, and the transport concentration of the fluidized solids c is defined by; $\varphi=(dV_v/dV)$, $c=(dV_{sf}/dV_v)$. Where dV indicates a volume element, dV_v the volume of interconnected void space of pores, which is fully occupied by the mixture of fluid and fluidized particles, and dV_{sf}, which indicates the volume of fluidized particles. It should be noticed that φ and c are functions of the location x_i and time t. The partial densities of the solid skeleton and fluidized particles are:

$$\rho'_s = (1-\varphi)\rho_s \qquad \rho'_{fs} = c\varphi\rho_s \tag{3}$$

Mass balances for the considered three-phase medium are given by the following expressions

$$\frac{\partial(c\varphi)}{\partial t} + \frac{\partial(cq_x)}{\partial x} = \frac{\partial \varphi}{\partial t} \qquad \frac{\partial q_x}{\partial x} = 0 \tag{4}$$

In the considered 1-D case, and due to the continuity, we have constant velocity along the length of the specimen, $q_x = q(t)$. The mass balance and the continuity are not sufficient for solving the problem of

ISSN 0148-9062

erosion since a constitutive law for erosion kinetics is needed to have a determined system. This is in general an evolution law for the porosity.

Probabilistic model for internal erosion kinetics

Let $p_{n|t}$ be the probability of a void to be at point n at time t and $q_{n|t}$ be the probability of a void to move from position n at time t. Then, the probability of a void to be at point n at time t+Δt is the sum of the probability of a void to be at the point n and not move, the probability of a void being able to move but having a particle in front of it and the probability of a particle be at point n and to move ahead (Figure 8).

$$p_{n|t+\Delta t} = P_{n|t}(1-q_{n|t}) + p_{n|t}q_{n|t}q_{n+1|t} + p_{n-1|t}q_{n-1|t}(1-p_{n|t}) \tag{5}$$

or

$$p + \frac{\partial p}{\partial t}\Delta t = p(1-q) + pq\left(p + \frac{\partial p}{\partial x}\Delta x\right) + \left(pq - \frac{\partial (pq)}{\partial x}\Delta x\right)(1-p) \tag{6}$$

Using the following identifications, $p \rightarrow \varphi/\varphi_{cr}$ and $q \rightarrow q_x\varphi$, Eqn. 6 leads to an evolution law for the porosity

$$\frac{\partial \varphi}{\partial t} = -\lambda q_x\left(\varphi - \frac{\varphi^2}{\varphi_{cr}}\right)\frac{\partial \varphi}{\partial x} \tag{5}$$

where λ has the dimension of inverse length and is probably related to the spatial frequency of the potential erosion starters points in the solid skeleton of the porous medium and must be determined experimentally. φ_{cr} is a critical value of φ for which the two competing phenomena, erosion and deposition, balance each other. Here $\varphi_{cr} = \varphi_{eq}$, taken from the measurements at the end of any constant flow-rate period. The constitutive Eqn. 7 is of the "divergence" type and differs from the one originally discussed in Vardoulakis *et al*. 1996, which had the character of an evolution equation

$$\frac{\partial \varphi}{\partial t} = \lambda q_x\left(\varphi - \frac{\varphi^2}{\varphi_{cr}}\right)c \tag{6}$$

Eqns 7 and 8 can be combined in a so-called "complete" constitutive equation of "balance-law" type, (Stavropoulou 1996), of the general form (where $\|q_x\|$ denotes the length of the vector).

$$\frac{\partial h_x}{\partial x} + g = 0 \qquad \text{where} \qquad h_x = (1-\varphi)q_x \qquad g = -\left(\varphi - \frac{\varphi^2}{\varphi_{cr}}\right)\frac{\partial \varphi}{\partial t} + c\|q_x\| \tag{7}$$

$$\frac{\partial \varphi}{\partial t} = \lambda\left(\varphi - \frac{\varphi^2}{\varphi_{cr}}\right)\left\{c\|q_x\| - \frac{\partial \varphi}{\partial x}q_x\right\} \tag{8}$$

ISSN 0148-9062

To cite this paper: Int. J. Rock Mech. & Min. Sci. 34:3-4, paper No. 292.

Numerical solution of density waves.

The constitutive Eqn 10 together with the mass balance Eqn 4 make-up a system of partial differential equations which can be solved numerically by the partial discretization procedure using the Finite Element Method in space and Finite Differences in time. The primary unknowns are the porosity φ and transport concentration c. This system is solved with given initial conditions for φ and c,$\varphi(x,0) = \varphi_0$ and $c(x,0) = c_o$ = 1.0e - 4, $\varphi(0,t) = \varphi_{cr}$, and $c(0,t) = c_o$, where c_o is a sufficiently small starter value. The result is insensitive to c_o as long as it is kept relatively small.

Back analysis: Danish beach sand

For the back analysis of the test on Danish beach sand, the above hydrodynamic model for grain transport with the following parameters was used; specimen length: *H=0.148 m,* initial porosity: φ_0*=0.343,* flow rate: *q=0.00027601 m/sec,* bulk density of solids: $\rho_s = 2650 kg/m^3$. The only remaining free constant is the parameter λ, which was selected as λ=90 m^{-1} so as to arrive at the simulation curves j = j(t) (Figure 9) and ; = ;(t) (Figure 11). The analysis was run for piecewise constant specimen length and for constant flow rate using a Galerkin-type Finite Element code developed in Stavropoulou.

In the Figures 9 and 10, the spatial profiles of the porosity and transport concentration are shown at various time steps. Figure 11 shows the motion of the density wave, which when it reaches the top of the sand body (free surface) the system tends to attain equilibrium. Furthermore, this figure demonstrates the mechanism of internal erosion: Increased fluid flow results into a mildly turbulent condition and to partial fluidization of the sand (c>0) so as 'waves' of fluidized particles move ahead. This has, as a result in the considered experiment, the rearrangement of sand grains and a net increase of porosity (Figure 12) and height of the specimen.

Back analysis: Valøygrind sand

For the back analysis of the column test with Valøygrind sand the following parameters are used; specimen length*: H=0.146 m,* initial porosity: φ_0*=0.34,* spatial frequency: λ*=150* m^{-1}*,* bulk density of solids: $\rho_s = 2650 kg/m^3$. The numerical results for the average density and the average porosity are compared with the measured average values in Figure 13 and Figure 14, repectively.

CONCLUSIONS

Sand production induced by fluid flow normal to the free surface has been investigated experimentally and theoretically. Linear flow experiments in unconsolidated sand has revealed a transient behaviour of the grain matrix in terms of induced density waves as a response to a perturbation of the fluid pressure field.

The observed phenomena were modelled through the use of Forcheimer's law for fluid flow, while an equation linear in porosity was formulated for the hydraulic resistivity. A non-linear law for the porosity evolution in time was established based on a probabilistic argument and previous work. In this constitutive equation the linear term in φ, the porosity, is responsible for the erosion, whereas the quadratic term in φ accounts for clogging and/or deposition phenomena. The observed erosion process can be explained by a density wave in unconsolidated sand as a result of change in the fluid flow rate. When the wave reaches the free surface the phenomenon stops to evolve and equilibrium is reached.

ISSN 0148-9062

To cite this paper: Int. J. Rock Mech. & Min. Sci. 34:3-4, paper No. 292.

As a general conclusion of this study in relation to sand production, we may say that changes in flow rate result temporally into mobilization of sand particles in form of transport concentration waves, which reach the free surface with some degree of diffusion.

ACKNOWLEDGMENTS

The authors wish to thank Norsk Hydro ASA, Statoil and IKU Petroleum Research for permission to publish the results. We will also thank Steinar Ommedal,Sintef Unimed, for operating the X-ray CT-scanner.

FIGURES

Paper 292, Figure 1.

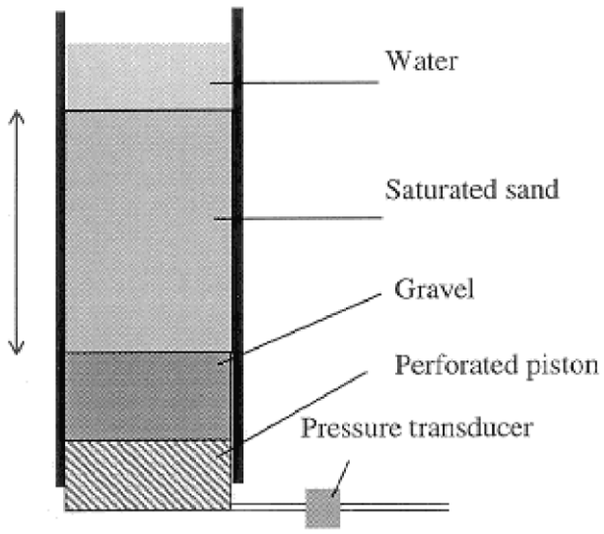

Figure 1. *Schematic illustration of the set-up for fluidized column experiment*

ISSN 0148-9062

To cite this paper: Int. J. Rock Mech. & Min. Sci. 34:3-4, paper No. 292.

Paper 292, Figure 2.

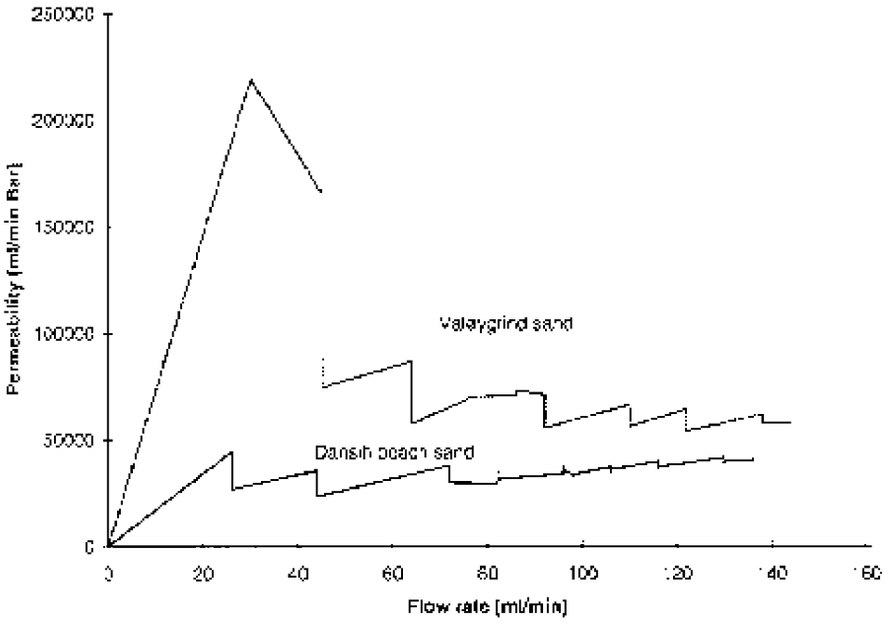

Figure 2. *The permeability variations in the two fluidized column tests.*

ISSN 0148-9062

To cite this paper: Int. J. Rock Mech. & Min. Sci. 34:3-4, paper No. 292.

Paper 292, Figure 3.

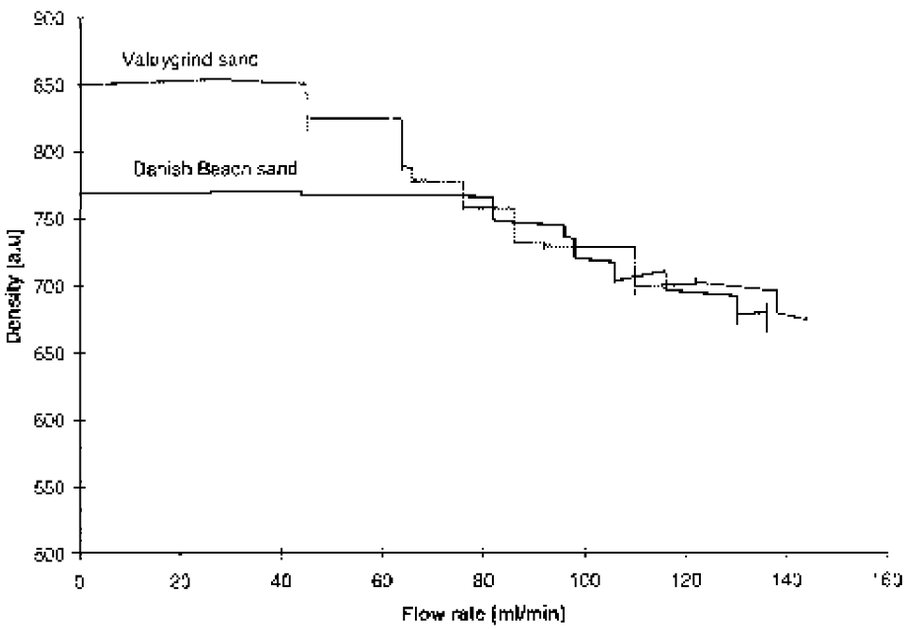

Figure 3. *The density variations in the two fluidized column tests.*

Paper 292, Figure 4.

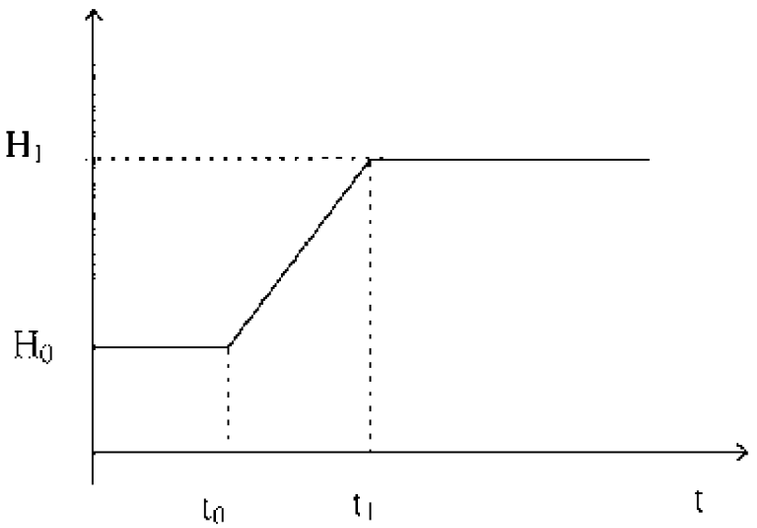

ISSN 0148-9062

To cite this paper: Int. J. Rock Mech. & Min. Sci. 34:3-4, paper No. 292.

Figure 4. *Principal illustration of the deformation process of the sand body due to increased fluid flow rate.*

Paper 292, Figure 5.

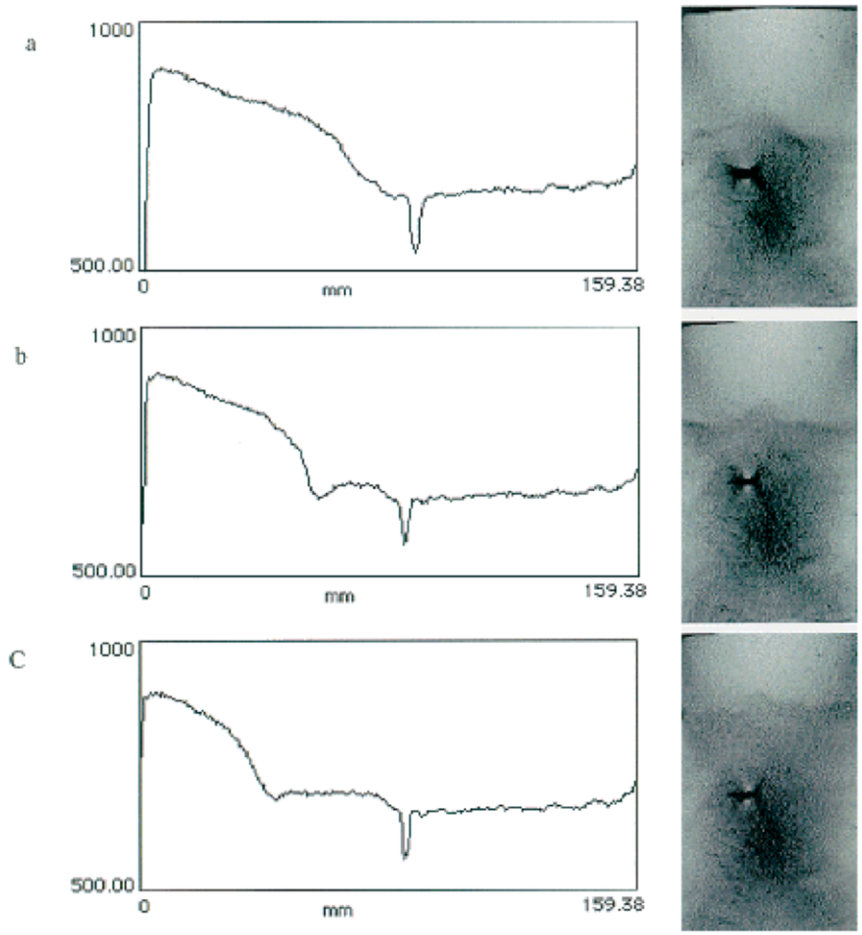

Figure 5. *Density variations along the sand body(a: image 6, b: image 7, c: image 8, Figure 6)*

ISSN 0148-9062

To cite this paper: Int. J. Rock Mech. & Min. Sci. 34:3-4, paper No. 292.

Paper 292, Figure 6.

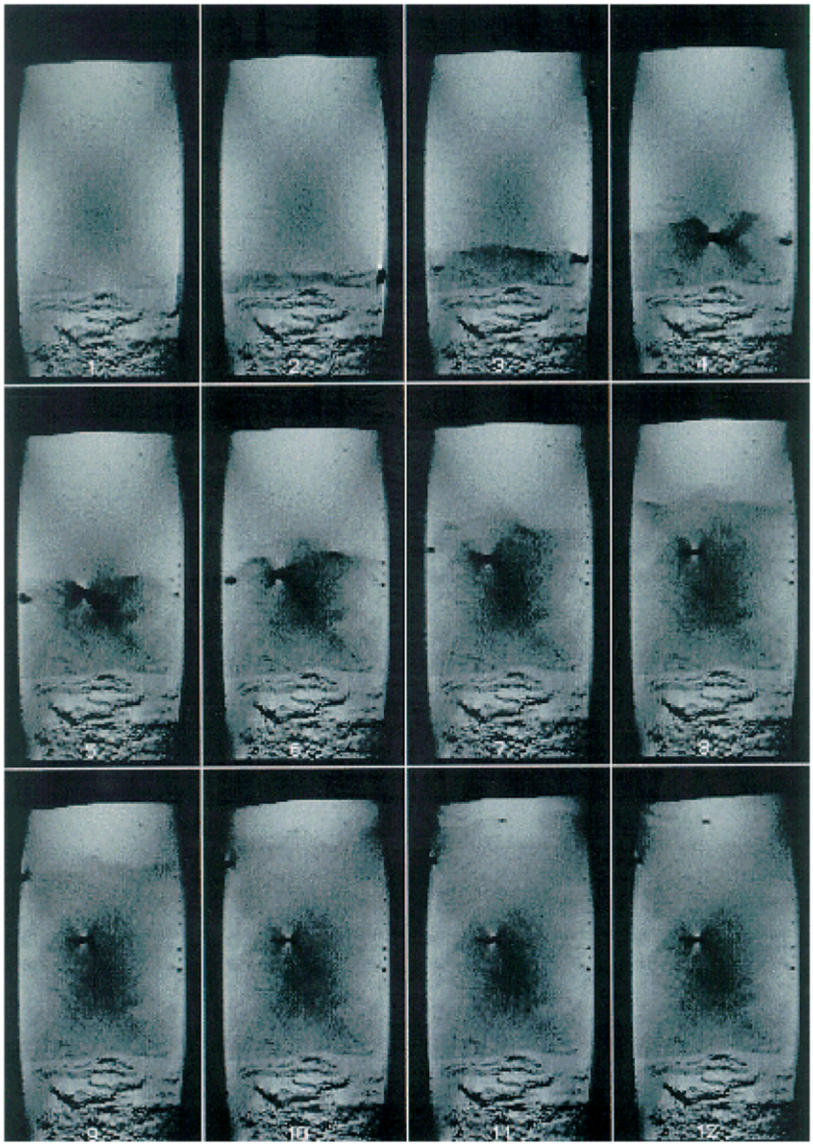

Figure 6. *X-ray tomography images from fluidized column experiments, illustration of the density wave.*

ISSN 0148-9062

To cite this paper: Int. J. Rock Mech. & Min. Sci. 34:3-4, paper No. 292.

Paper 292, Figure 7.

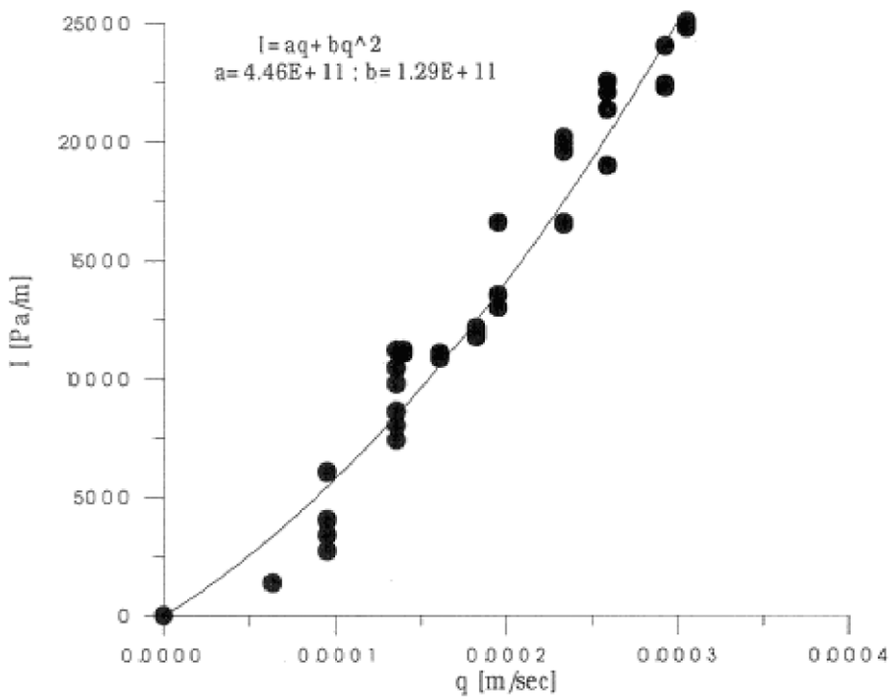

Figure 7. *Calibration of Forcheimer's law.*

Paper 292, Figure 8.

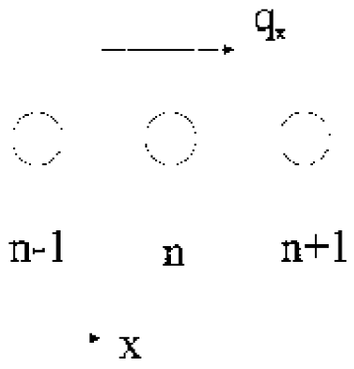

Figure 8. *Motion of voids*

ISSN 0148-9062

To cite this paper: Int. J. Rock Mech. & Min. Sci. 34:3-4, paper No. 292.

Paper 292, Figure 9.

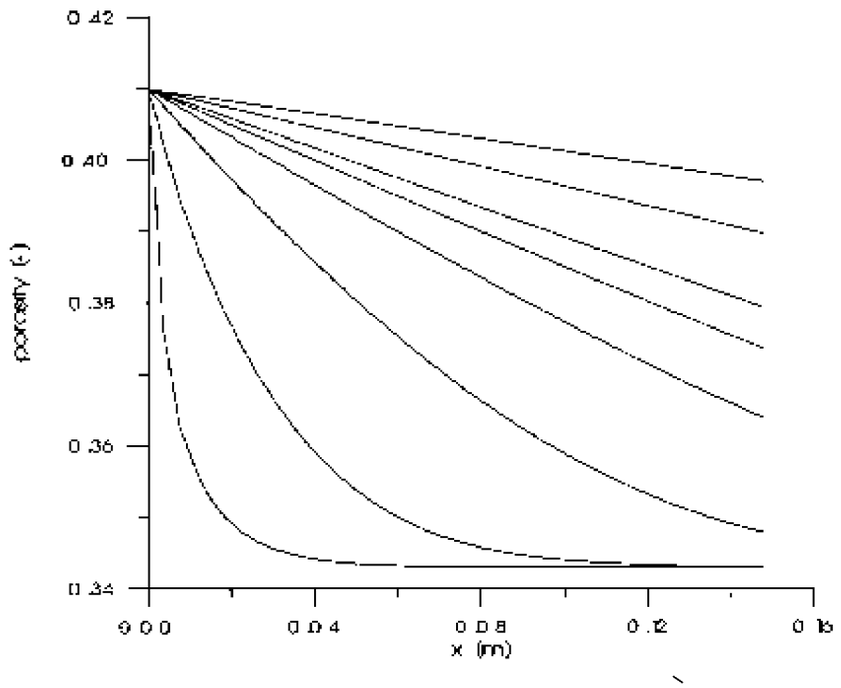

Figure 9. *Spatial profiles of porosity at various time steps (Danish beach sand).*

ISSN 0148-9062

To cite this paper: Int. J. Rock Mech. & Min. Sci. 34:3-4, paper No. 292.

Paper 292, Figure 10.

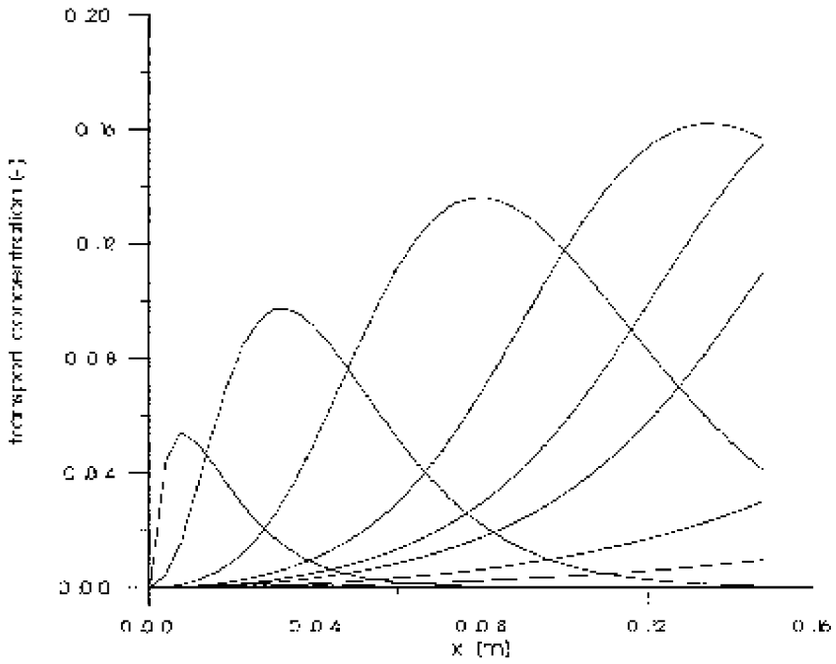

Figure 10. *Sand-wave curve spatial profiles of transport concentration at various time steps (Danish beach sand).*

ISSN 0148-9062

To cite this paper: Int. J. Rock Mech. & Min. Sci. 34:3-4, paper No. 292.

Paper 292, Figure 11.

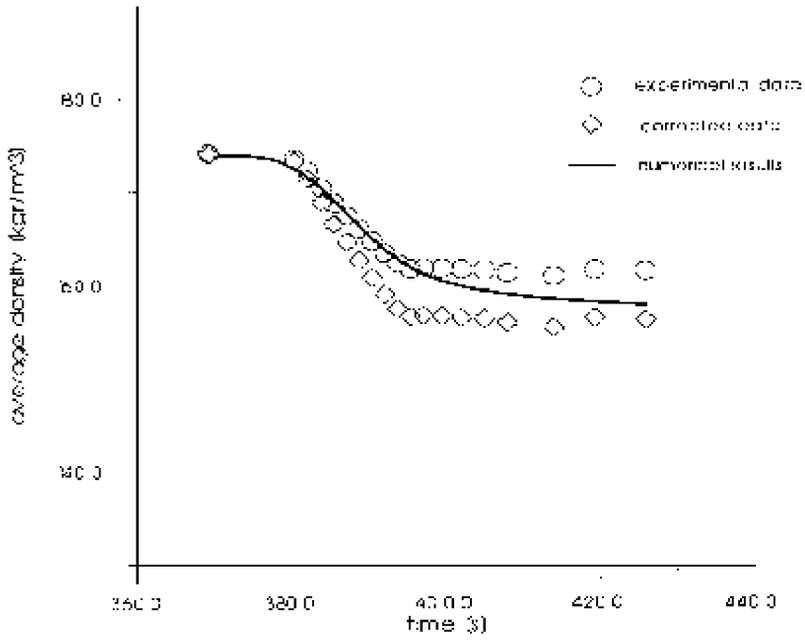

Figure 11. *Time evolution of average density (Danish beach sand).*

ISSN 0148-9062

To cite this paper: Int. J. Rock Mech. & Min. Sci. 34:3-4, paper No. 292.

Paper 292, Figure 12.

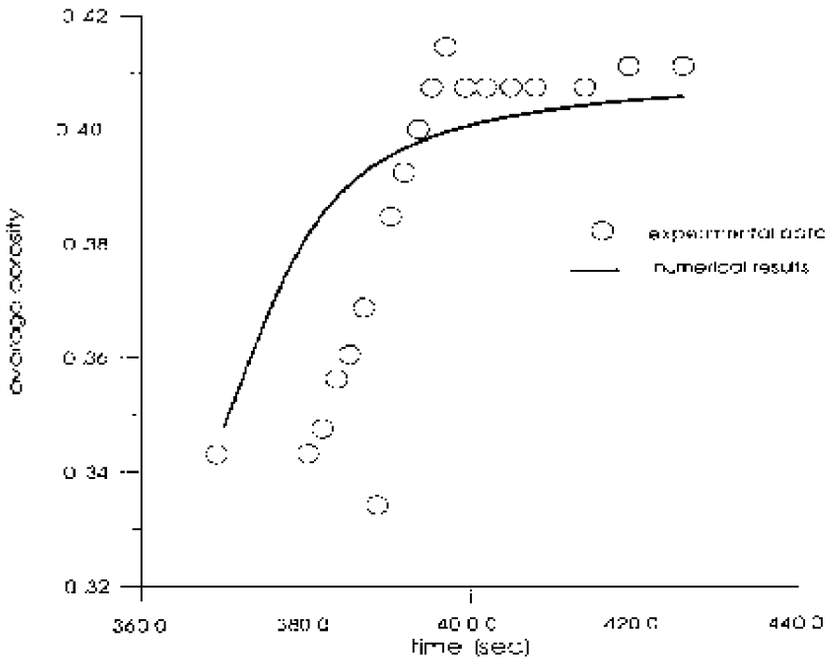

Figure 12. *Time evolution of average porosity (Danish beach sand).*

ISSN 0148-9062

To cite this paper: Int. J. Rock Mech. & Min. Sci. 34:3-4, paper No. 292.

Paper 292, Figure 13.

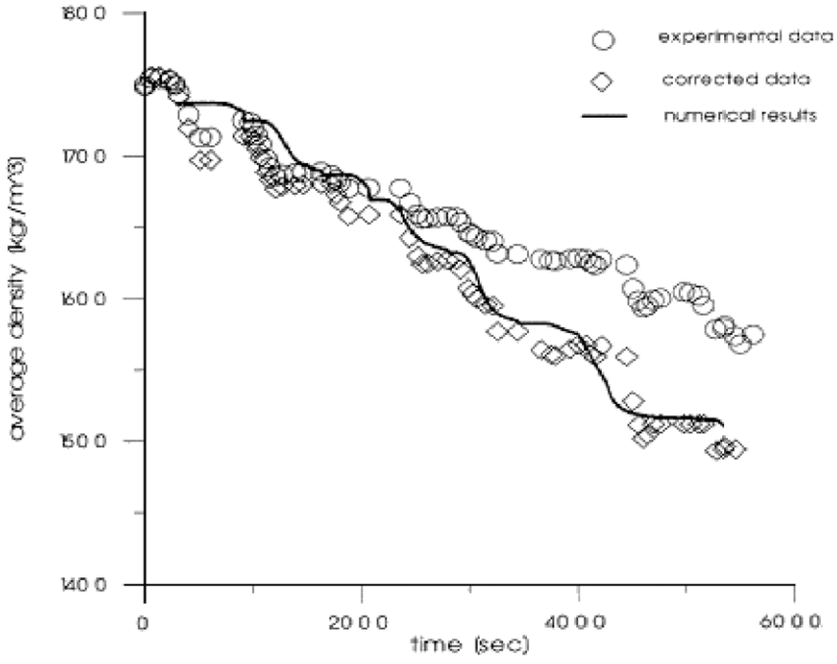

Figure 13. *Predicted and measured average density evolution.*

ISSN 0148-9062

To cite this paper: Int. J. Rock Mech. & Min. Sci. 34:3-4, paper No. 292.

Paper 292, Figure 14.

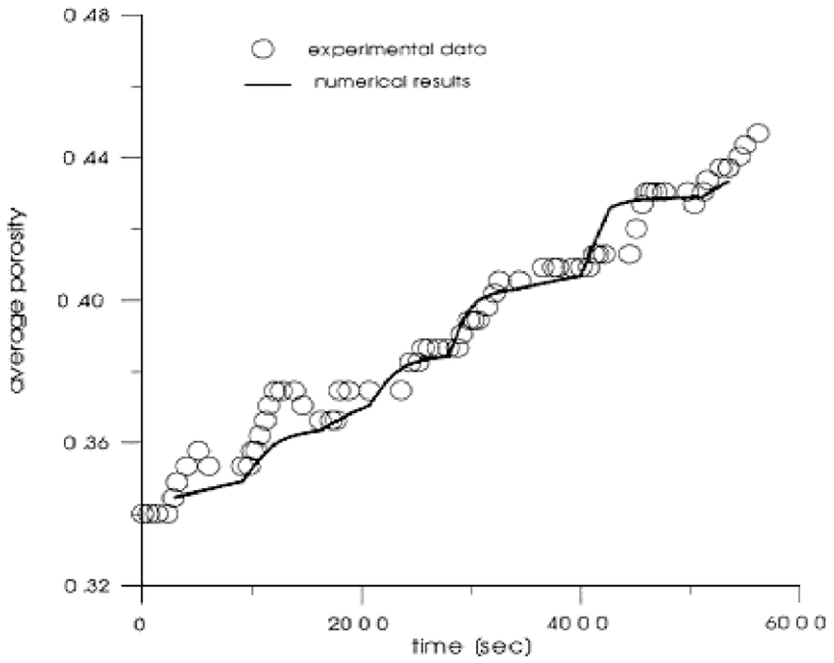

Figure 14. *Predicted and measured average porosity evolution.*

References

References

Stavropoulou M. 1996: Coupled hydromechanical instabilities in deep boreholes, Ph. D. thesis, National Technical University of Athens, Greece.

Vardoulakis I., Stavropoulou M., Papanastasiou P. 1996, Hydromechanical aspects of sand production problem, *Transport in Porous Media,* **22,** 225–244.

Tronvoll J. 1993: Investigation of cavity failures for sand production prediction.. Ph. D. thesis, The Norwegian Institute of Technology, Trondheim

Vardoulakis I., Sulem J. 1995: *Bifurcation Analysis in Geomechanics,* Sect. 5.6.3., Blackie Academic and Professional.

ISSN 0148-9062